Spin-Orbit Splitting in Single-Layer MoS_2 Revealed by Triply Resonant Raman Scattering

Linfeng Sun,[1] Jiaxu Yan,[1] Da Zhan,[1,2,*] Lei Liu,[3] Hailong Hu,[1,2] Hong Li,[4] Ben Kang Tay,[4] Jer-Lai Kuo,[5] Chung-Che Huang,[6] Daniel W. Hewak,[6] Pooi See Lee,[2] and Ze Xiang Shen[1,2,†]

[1]*Centre for Disruptive Photonic Technologies, School of Physical and Mathematical Sciences, Nanyang Technological University, Singapore 637371, Singapore*

[2]*Division of Materials Technology, School of Materials Science and Engineering, Nanyang Technological University, Singapore 639798, Singapore*

[3]*Key Laboratory of Luminescence and Applications, CIOMP, Chinese Academy of Sciences, Changchun 130033, People's Republic of China*

[4]*Microelectronics Centre, School of Electrical and Electronic Engineering, Nanyang Technological University, Singapore 639798, Singapore*

[5]*Institute of Atomic and Molecular Sciences, Academia Sinica, Taipei 10617, Taiwan*

[6]*Optoelectronics Research Centre, University of Southampton, Southampton SO17 1BJ, United Kingdom*

(Received 9 May 2013; published 17 September 2013)

Although new spintronic devices based on the giant spin-orbit splitting of single-layer MoS_2 have been proposed, such splitting has not been studied effectively in experiments. This Letter reports the valence band spin-orbit splitting in single-layer MoS_2 for the first time, probed by the triply resonant Raman scattering process. We found that upon 325 nm laser irradiation, the second order overtone and combination Raman modes of single-layer MoS_2 are dramatically enhanced. Such resonant Raman enhancement arises from the electron-two-phonon triple resonance via the deformation potential and Fröhlich interaction. As a sensitive and precise probe for the spin-orbit splitting, the triply resonant Raman scattering will provide a new and independent route to study the spin characteristics of MoS_2.

DOI: 10.1103/PhysRevLett.111.126801 PACS numbers: 73.22.Pr, 61.48.Gh, 68.35.B−

Recently, layered semiconductor molybdenum disulfide (MoS_2) has created an intense surge in research activities due to the existence of an intrinsic band gap [1–4]. The single-layer MoS_2 presents a direct band gap at the K point of the Brillouin zone, which is distinct from its few-layer and bulk cases with an indirect band gap [5,6]. This crossover of band gap in single-layer MoS_2 gives rise to its exotic electronic and optical properties [1,2,7]. For example, a single-layer MoS_2 transistor has been realized which exhibits a high current on-off ratio and mobility that is comparable to transistors made of silicon films and better than that from graphene ribbons [1,8,9]. In addition, a direct transition in the visible range makes it favorable for potential applications in optoelectronic devices. Another significant physical characteristic in single-layer MoS_2 is a sizable spin-orbit (SO) splitting due to the absence of inversion symmetry. The strong SO splitting breaks the degeneracy of the valence band maximum and conduction band minimum along the direction Γ-K [10]. This splitting makes it desirable for the realization of many physical phenomena such as the spin-Hall effect [11], quantum spin-transfer [12], spin domain reversal [13], and magnetic phase transition [14], which are promising for their potential applications in spin electronics and quantum information processing and so on [15]. Due to the crucial role of SO coupling in controlling the spins of carriers in spintronic-based devices, one important challenge is to develop an experimental method effectively, to detect and explore intrinsic SO coupling in MoS_2.

Previous attempts to explore SO coupling were mainly concerned with the energy difference between the two so-called A and B exciton peaks in the photoluminescence (PL) of MoS_2 [5,6]. However, the identification of these two excitons is still unsettled because of the involvement of an additional bound exciton peak, which is sensitive to the ambient environment [16,17]. Occasionally, only one PL peak is detected at the room temperature for single-layer MoS_2 due to the quenching effect of bound excitons [5,18]. Furthermore, the energy difference between A and B excitons does not show obvious layer dependence in the PL spectrum, which is in conflict with the calculation results. On the other hand, the resonant Raman spectrum is very sensitive to the matching between the valence band splitting and the energy of the phonons involved. To shed light on the SO coupling in MoS_2, the resonance Raman scattering, by exploring a specific excitation wavelength, would be an efficient and accurate method.

In this Letter, we used four excitation laser lines to systematically investigate the second order and combination Raman modes in MoS_2, including single-layer, bilayer, quad-layer, and bulk MoS_2 as reference samples. Under 325 nm laser excitation, the intensities of high-order modes ($2E^1_{2g}$ and $2A_{1g}$) are dramatically enhanced in few-layer MoS_2 compared with those using other laser lines. Here, the Raman resonance behavior observed is ascribed to the electron-two-phonon coupling based triply resonant Raman scattering (TRRS) process, in which the existence of SO splitting provides a pathway for the resonance of

overtone and combination phonon modes. In contrast, we did not observe the prominent high-order Raman peaks in bulk MoS_2 due to its larger value of SO splitting which does not match the energy of the involved phonons. The laser-selective Raman enhancement for overtone and combination phonon modes leads to a new method for probing the SO splitting in single-layer MoS_2, which is critically lacking in MoS_2-based spintronic devices.

The samples were prepared from natural MoS_2 crystal (SPI Supplies) by mechanical exfoliation on silicon wafers covered by 285 nm thick SiO_2. The numbers of MoS_2 layers were first identified by Raman spectra and then confirmed by atomic-force microscopy, which is consistent with previous results [3]. The Raman measurement with a 488 nm laser line was conducted by a WITEC alpha 300R Confocal Raman microscope with 1800 mm^{-1} grating and the measurement under 457 nm laser excitation was conducted by a WITEC alpha 200R with the same systematic integration and measurement parameters. Raman spectra excited by 325 and 532 nm lasers were performed using a Renishaw Invia Raman microscope. The powers of all laser lines used in our experiment were kept well below 0.5 mW to avoid heating effects.

Figure 1 shows the Raman spectra of the MoS_2 samples with the different thicknesses excited by various excitation lasers. Obviously, the intensities of the three high-order modes excited by the 325 nm laser are enhanced dramatically. These three Raman peaks with prominent intensities are observed in the range from 750 to 840 cm^{-1}, which have been assigned as the second order and combination modes of E^1_{2g} and A_{1g} [19,20]. Unlike the 325 nm laser case, only first-order modes (E^1_{2g} and A_{1g}) can be obviously observed when the samples are excited by the 457, 488, and 532 nm lasers. We attribute this intensity enhancement of the observed high-order modes to the electron-two-phonon involved TRRS process [21–23]. As illustrated in Fig. 2(b), four steps are involved in this process: (1) an electron is excited resonantly from the v_2 band to the conduction band (schematically represented by c_i) by absorbing a photon; (2) the hole in the v_2 band is scattered by a phonon with momentum q to the v_1 band via an interband transition; (3) another phonon with momentum $-q$ scatters the hole to the top of the v_1 band via an intraband transition process; (4) the electron-hole pair recombines at the top of the v_1 band and a photon is emitted during this recombination process. The energy difference between the laser and the emitted photon is equal to the value of the energy splitting $\Delta E_{SO} = E(v_1)–E(v_2)$. In the case of single-layer MoS_2, ΔE_{SO} comes exclusively from spin-orbit coupling. The key factor to fulfill the TRRS conditions is that ΔE_{SO} has to match the sum of two involved first-order phonon energies well. ΔE_{SO} is a result of the lack of inversion symmetry in single-layer MoS_2 [Fig. 2(a)], while for the bilayer case, where it possesses inversion symmetry, the valence band also splits due to the combination effects of SO coupling and interlayer coupling [24]. For the resonant Raman observed in MoS_2, we need to address two issues: (1) How does the valence (conduction) band split? (2) Which electronic transition is allowed between the valence and conduction band using 325 nm laser excitation?

We have calculated the electronic band structures by considering SO coupling for MoS_2 layers with different thicknesses using the Vienna *ab initio* simulation package (VASP), within the local-density approximation [25,26]. The cutoff energy for the basis set was 400 eV.

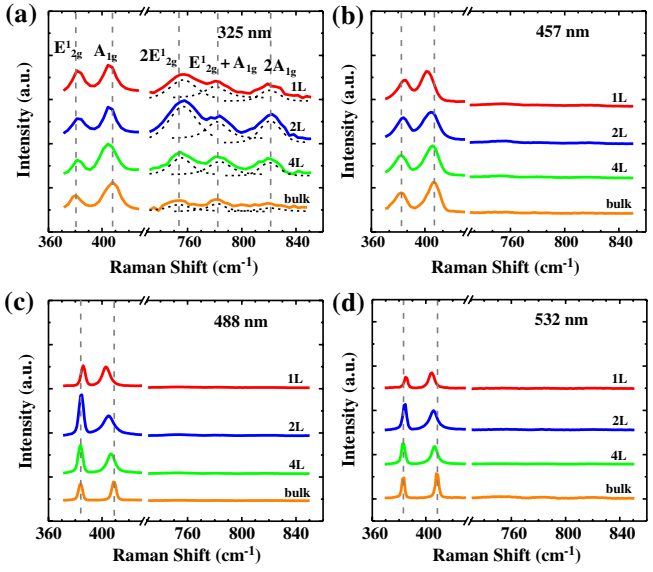

FIG. 1 (color online). The Raman spectra of MoS_2 samples with different thicknesses excited by (a) 325, (b) 457, (c) 488, and (d) 532 nm laser lines, respectively. All the Raman spectra have been normalized by the intensity of the A_{1g} peak. The dashed Raman spectra in Fig. 1(a) represent the fitting curves. The vertical dashed lines represent the peak positions of the bulk samples.

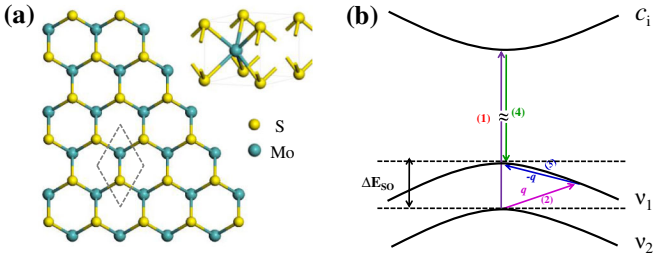

FIG. 2 (color online). (a) Schematic of MoS_2 monolayer structure (left). The black lines indicate the unit cell in the *ab* plane. The unit cell (right) for the monolayer clearly shows the spatial inversion symmetry breaking in the monolayer. (b) Schematic diagram for the TRRS process in MoS_2, where v_1, v_2 represent the valence band splitting due to spin-orbit interaction, and c_i represents a conduction band. Detailed discussion on the conduction band splitting and their involvement in the TRRS process is given in the text and in Fig. 3.

The Brillouin-zone integration was performed within the Monkhorst-Pack scheme using a $36 \times 36 \times 1$ mesh. The energy relaxation for each strain step is continued until the forces on all the atoms are converged to less than 10^{-2} eV^{-1}. The calculations considering SO coupling effects are performed in the noncollinear mode implemented in VASP by Kresse and Lebacq [27]. Clearly, the valence band in each electronic band shown in Fig. 3 splits into two bands marked as v_1 and v_2 bands at the top of the valence band. Furthermore, the conduction band at around 3.7 eV also splits into c_5 and c_6.

To determine exactly which transition ($v_{1(2)}$ to $c_{5(6)}$ bands) is allowed, we need to consider the spin indexes of these four involved electronic bands. Only transitions of the same spin are allowed. The red and blue lines in Fig. 3(a) indicate the spin-up and spin-down states, respectively, where both transitions from v_2 to c_6 bands and from v_1 to c_5 are allowed. When excited by a 325 nm laser, its photon energy ($\sim$3.81 eV) matches well with that of the v_2 to c_6 electronic transition (3.87 eV) but it does not match as well for the v_1 to c_5 transition (3.62 eV). The purple arrows in Fig. 3 show the permitted v_2 to c_6 electronic transition.

To further check whether this transition (v_2 to c_6) conforms to the selection rule, we have calculated the partial charge density of the involved bands in Fig. 4. The valence band maximum (v_1 and v_2 bands) in single-layer MoS_2 is mainly contributed by d orbitals of Mo atoms, which is consistent with previous reports [10,17,28]. For conduction bands c_5 and c_6, the former is mainly originated from the d orbitals of Mo atoms while the latter arises from both the contribution of d orbitals of Mo atoms and the p orbitals of S atoms. As electronic transition requires that the difference of the azimuthal quantum number must be 1, the only allowed electronic transition is that from the Mo d orbitals in the v_2 band to the S p orbital in the c_6 band. This transition from the v_2 to c_6 band together with the spin valley coupling could be further studied by optical helicity as the transitions from v_1 and v_2 to c_6 band are attributed to α and β excitons [29], which is beyond the scope of this article and will be addressed elsewhere.

Thus, a whole physical picture for the TRRS process emerges: First, an electron is excited from the v_2 band to the c_6 band by absorbing a photon at the K point of the Brillouin zone; Then, the hole in the v_2 band is scattered by a phonon with momentum q to the v_1 band by interband transition as a consequence of deformation potential interaction [30]; Another phonon with momentum $-q$ scatters the hole to the top of the v_1 band by intraband transition to form an exciton with the electron in the c_6 band due to the Fröhlich interaction [31]; Finally, the electron-hole pair recombines at the top of the v_1 band and a photon is emitted during this recombination process. It is worth noting that for fulfilling the Raman enhancement of the second order modes ($2E^1_{2g}$), the Fröhlich interaction induced electron scattering by an E^1_{2g} phonon must be involved. Otherwise, the Raman intensity of the $2E^1_{2g}$ mode cannot be enhanced [21,23]. Therefore, the electron-two-phonon coupling in this TRRS process is dominated by the deformation potential interaction induced interband transition and Fröhlich interaction induced intraband transition. For the energy and momentum conservation in Raman scattering, the energy transitions of these three different modes can be written as equations (1)–(3), respectively:

$$E_{\text{laser}} = E_{\text{exciton}} + 2E_{E^1_{2g}}, \tag{1}$$

$$E_{\text{laser}} = E_{\text{exciton}} + 2E_{A_{1g}}, \tag{2}$$

$$E_{\text{laser}} = E_{\text{exciton}} + E_{E^1_{2g}} + E_{A_{1g}}. \tag{3}$$

In each case, the overall momentum of the two involved phonons must be zero in order to satisfy momentum conservation. Note that both the E^1_{2g} and A_{1g} modes are almost dispersionless in momentum space along the Γ-M direction in momentum space [32–34]. This particular characteristic is very useful for observing the strong TRRS in our

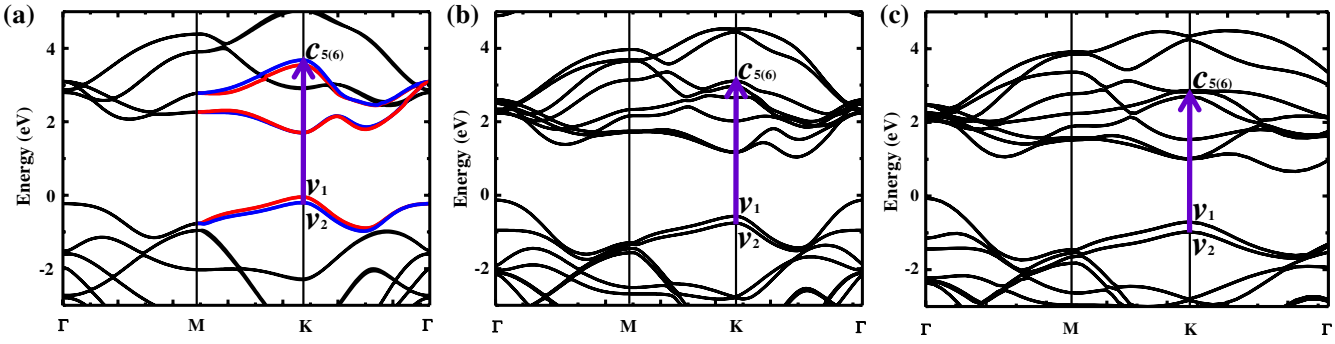

FIG. 3 (color online). The calculated electronic band structures of MoS_2 with the SO coupling considered: (a) single layer, (b) bilayer, and (c) bulk. The red (v_1 and c_5) and blue lines (v_2 and c_6) represent the spin-up and spin-down states, respectively. The purple arrow in each graph represents the 325 nm laser induced electronic transition from v_2 to c_6 bands as described in the process (1) in Fig. 2(b). Here we only show the positive helicity (σ_+) case, as an example.

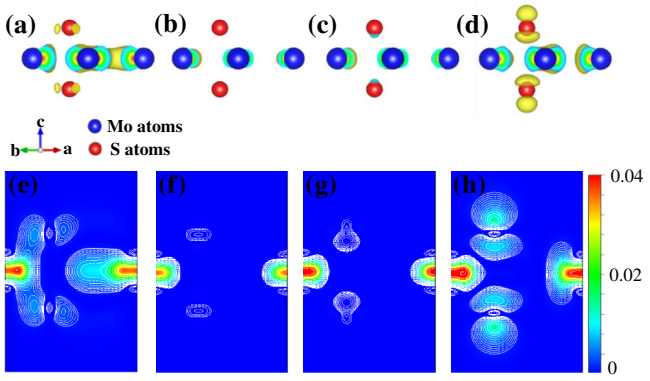

FIG. 4 (color online). (a)–(d) 3D partial charge density of electronic bands (a) v_2, (b) v_1, (c) c_5, and (d) c_6 for single-layer MoS_2, respectively. (e)–(h) 2D partial charge density graphs corresponding to the four electronic bands in (a)–(d).

experiments. The TRRS process requires both energy and momentum conservation. As shown in process 2 in Fig. 2(b), the phonon participating in the TRRS must have the right energy ($\Delta E_{SO}/2$) and the right momentum q simultaneously to scatter the hole from the v_2 band to the v_1 band. The flat phonon dispersion curve in MoS_2 means that there exist many phonons with similar energy but very different momentum. Once the phonon energy matches the right energy, it is always possible to find a phonon with the suitable momentum to ensure momentum conservation. The same holds true for process 3 in Fig. 2(b) as well.

The experimental observation of TRRS for second order and combination modes is a significant step towards exploring the value of SO splitting in single-layer MoS_2. Previous calculations using Perdew-Burke-Ernzerhof, Heyd-Scuseria-Ernzerhof, and GW approximation have been performed to obtain the value of SO splitting but yielded varying results between 146 and 193 meV [35]. Our calculation results show that the splitting of 152 meV is within the range reported in the literature. In our experiment, when excited by the 325 nm laser, three resonant high-order peaks due to TRRS were observed with phonon energies between 93 meV ($2E^1_{2g}$) and 102 meV ($2A_{1g}$), giving a SO splitting value of about 100 meV for single-layer MoS_2. The origin of band splitting in bilayer MoS_2 differs from the single-layer case as we discussed before, although the splitting value is comparable (154 meV for single layer and 184 meV for bilayer as reported by theoretical calculation results [35,36]). For the bilayer case, the splitting arises from a combination of SO coupling and interlayer coupling. However, the spin is degenerate at the top of valence bands because of the inversion and time reversal symmetry, which means each valence band (v_1 or v_2) at k and k' valley contains both spin-up and spin- down states where different spin-polarized states come from different individual layers. Thus, the interlayer coupling within the same spin states needs to commute with SO splitting [37]. The bulk MoS_2 possesses much larger splitting of the valence band [Fig. 3(c)], which means that the probability of TRRS is reduced due to the loss of energy match between splitting of the valence bands and energy of the two phonons involved. As the intensities of the second order and combination Raman modes in TRRS are very sensitive to the energy splitting between v_1 and v_2 bands, we observe much weaker intensities of overtone and combination modes in bulk MoS_2.

In summary, we have experimentally observed the resonant enhancement of the second order and combination Raman modes in few-layer MoS_2 excited by a 325 nm laser. Combining the first-principles calculation with considering SO coupling effects, it is revealed that the Raman enhancement is due to the Fröhlich-interaction and deformation potential-interaction involved electron-two-phonon TRRS process. The SO splitting at the top of the valence band serves as an essential prerequisite for high-order Raman mode resonance. Particularly, by the triply resonant Raman effect, we defined the value of SO splitting in the single-layer MoS_2 experimentally, which is consistent with our calculation results. Given the giant SO splitting in single-layer MoS_2, the 325 nm laser-based TRRS technique will provide a new and convenient way to investigate the SO splitting in MoS_2, which is of great importance for developing the MoS_2-based spintronic devices of the future [17,36].

L. S. and J. Y. contributed equally to this work.

*physicsor@gmail.com
†zexiang@ntu.edu.sg

[1] B. Radisavljevic, A. Radenovic, J. Brivio, V. Giacometti, and A. Kis, Nat. Nanotechnol. **6**, 147 (2011).
[2] Q. H. Wang, K. Kalantar-Zadeh, A. Kis, J. N. Coleman, and M. S. Strano, Nat. Nanotechnol. **7**, 699 (2012).
[3] C. Lee, H. Yan, L. E. Brus, T. F. Heinz, J. Hone, and S. Ryu, ACS Nano **4**, 2695 (2010).
[4] H. S. S. Ramakrishna Matte, A. Gomathi, A. K. Manna, D. J. Late, R. Datta, S. K. Pati, and C. N. R. Rao, Angew. Chem., Int. Ed. Engl. **49**, 4059 (2010).
[5] K. F. Mak, C. Lee, J. Hone, J. Shan, and T. F. Heinz, Phys. Rev. Lett. **105**, 136805 (2010).
[6] A. Splendiani, L. Sun, Y. Zhang, T. Li, J. Kim, C.-Y. Chim, G. Galli, and F. Wang, Nano Lett. **10**, 1271 (2010).
[7] H. Wang, L. Yu, Y. H. Lee, Y. Shi, A. Hsu, M. L. Chin, L. J. Li, M. Dubey, J. Kong, and T. Palacios, Nano Lett. **12**, 4674 (2012).
[8] X. Li, X. Wang, L. Zhang, S. Lee, and H. Dai, Science **319**, 1229 (2008).
[9] L. Gomez, I. Aberg, and J. L. Hoyt, IEEE Electron Device Lett. **28**, 285 (2007).
[10] Z. Y. Zhu, Y. C. Cheng, and U. Schwingenschlögl, Phys. Rev. B **84**, 153402 (2011).
[11] J. E. Hirsch, Phys. Rev. Lett. **83**, 1834 (1999).
[12] L. Berger, Phys. Rev. B **54**, 9353 (1996).
[13] A. Chernyshov, M. Overby, X. Liu, J. K. Furdyna, Y. Lyanda-Geller, and L. P. Rokhinson, Nat. Phys. **5**, 656 (2009).

[14] J. Zhang *et al.*, Science **339**, 1582 (2013).
[15] F. Pulizzi, Nat. Mater. **11**, 367 (2012).
[16] G. Sallen *et al.*, Phys. Rev. B **86**, 081301 (2012).
[17] K. F. Mak, K. He, J. Shan, and T. F. Heinz, Nat. Nanotechnol. **7**, 494 (2012).
[18] T. Korn, S. Heydrich, M. Hirmer, J. Schmutzler, and C. Schuller, Appl. Phys. Lett. **99**, 102109 (2011).
[19] J. M. Chen and C. S. Wang, Solid State Commun. **14**, 857 (1974).
[20] A. M. Stacy, and D. T. Hodul, J. Phys. Chem. Solids **46**, 405 (1985).
[21] A. Alexandrou, Y. Pusep, and M. Cardona, Phys. Rev. B **39**, 8308 (1989).
[22] A. Alexandrou, C. Trallero-Giner, A. Cantarero, and M. Cardona, Phys. Rev. B **40**, 1603 (1989).
[23] A. Alexandrou and M. Cardona, Solid State Commun. **64**, 1029 (1987).
[24] T. Cheiwchanchamnangij and W. R. L. Lambrecht, Phys. Rev. B **85**, 205302 (2012).
[25] G. Kresse and J. Furthmuller, Phys. Rev. B **54**, 11169 (1996).
[26] G. Kresse and J. Furthmuller, Comput. Mater. Sci. **6**, 15 (1996).
[27] D. Hobbs, G. Kresse, and J. Hafner, Phys. Rev. B **62**, 11556 (2000).
[28] W. Feng, Y. Yao, W. Zhu, J. Zhou, W. Yao, and D. Xiao, Phys. Rev. B **86**, 165108 (2012).
[29] P. V. Kasowski, Phys. Rev. Lett. **30**, 1175 (1973).
[30] D. A. Kleinman, R. C. Miller, and A. C. Gossard, Phys. Rev. B **35**, 664 (1987).
[31] F. Cerdeira, E. Anastassakis, W. Kauschke, and M. Cardona, Phys. Rev. Lett. **57**, 3209 (1986).
[32] K. Kaasbjerg, K. S. Thygesen, and K. W. Jacobsen, Phys. Rev. B **85**, 115317 (2012).
[33] B. Chakraborty, H. S. S. Ramakrishna Matte, A. K. Sood, and C. N. R. Rao, J. Raman Spectrosc. **44**, 92 (2013).
[34] A. Molina-Sanchez and L. Wirtz, Phys. Rev. B **84**, 155413 (2011).
[35] A. Ramasubramaniam, Phys. Rev. B **86**, 115409 (2012).
[36] D. Xiao, G. B. Liu, W. Feng, X. Xu, and W. Yao, Phys. Rev. Lett. **108**, 196802 (2012).
[37] H. Zeng *et al.*, Sci. Rep. **3**, 1608 (2013).